International Journal of Heat and Mass Transfer 184 (2022) 122357

Contents lists available at ScienceDirect

International Journal of Heat and Mass Transfer

journal homepage: www.elsevier.com/locate/hmt

Investigation of microscopic mechanisms for water-ice phase change propagation control

Yu-Kai Weng, Seungha Shin*, Kenneth D. Kihm, Mohammad Bahzad, Douglas S. Aaron

Department of Mechanical, Aerospace, and Biomedical Engineering, The University of Tennessee, Knoxville, TN, 37996, United States of America

ARTICLE INFO

Article history:
Received 1 August 2021
Revised 23 November 2021
Accepted 30 November 2021
Available online 11 December 2021

Keywords:
Water freezing
Graphene structuring
Surface interaction
Molecular dynamics

ABSTRACT

The influence of thermodynamic and structural conditions on water-ice phase change process was investigated with consideration of graphene-water surface interactions for fundamental understanding and effective control of freezing propagation. The phase change propagation as well as structural and energetic properties during the phase change were examined by analyzing atomic data from molecular dynamics simulations. The freezing propagation speed is affected by the competition between atomic mobility and thermodynamic driving force for phase change, which causes an optimal temperature for fast ice growth to appear at 252 K. In addition, the water-ice interfacial energy, which depends on the orientation of the water-contacting ice surface, changes interfacial structural stability and thus freezing propagation, i.e., a higher interfacial energy leads to a faster ice propagation. Therefore, we suggest that the water-ice phase change propagation can be controlled by adjusting the orientation of ice crystal. The surface interactions, or graphene-water interactions in this research, affect the energetics near the water-surface interface. The energetic change rearranges the ice crystal or surface structures to reach the most stable ice-surface configuration or minimum energy state, in which the basal plane of the ice crystal is parallel with the graphene surface. As ice propagation is the slowest perpendicular to the basal plane, ice can grow faster parallel to graphene surface. The findings from this study provides insights to ice propagation control mechanisms for versatile freeze casting and its broader applications.

1. Introduction

Water freezing is one of the most familiar phase-change phenomena in nature and an essential process for diverse science and engineering fields, such as microbiology [1], physics [2], and materials science [3]. One of the representative applications, which take advantage of the water-ice phase change process, is freeze casting or ice templating, where materials dispersed in liquid can be aligned by the anisotropic solidification of the liquid [4]. Freeze casting is employed to produce aligned porous structure from various building blocks [5], such as ceramics [6], graphene [7], and carbon nanotubes [8]. We studied the freezing process with an interest in the synthesis of graphene aerogels with aligned pores, which can be used as a component of electrochemical storage systems, specifically as an electrode material in organic redox flow batteries [9]. Since the working principle of freeze casting is to construct the material by phase change of water, water-ice interface propagation behaviors affect the resulting structure. For example, the average pore size and wall thickness of porous structures manufactured by freeze casting can be controlled by the solidification velocity [10]. Therefore, investigation of effective control of ice front propagation is essential for the control of freeze-cast material structures and ultimately their application performance.

Previous studies reported that the thermodynamic driving force for phase change and the self-diffusivity of water molecules have an opposite dependency on the temperature in the supercooling region [11, 12]. Thus, temperature can be one of the parameters controlling ice growth rate [13]. Surface interaction can be another possible parameter to control ice propagation, as it was reported to change the ice crystal structure in the proximity of surface/water interface [14], which can also alter the ice propagation and freeze-cast structures. For example, if a droplet of water was frozen between two layers of graphene, a two-dimensional (2D) square-like crystal ice structure formed [15]. Since the interaction between water and graphene enhances the reordering of the water molecules [16], the freezing behavior and water-ice interface propagation near the graphene appear differently such as crystal structure [17]. Moreover, the average density profile and diffusion of water molecules near the interface can be changed by the crystal orientation of ice surface [18] in contact with water. Therefore, we can expect the control of water-ice interface propagation to be

* Corresponding author.
E-mail address: sshin@utk.edu (S. Shin).

https://doi.org/10.1016/j.ijheatmasstransfer.2021.122357
0017-9310/

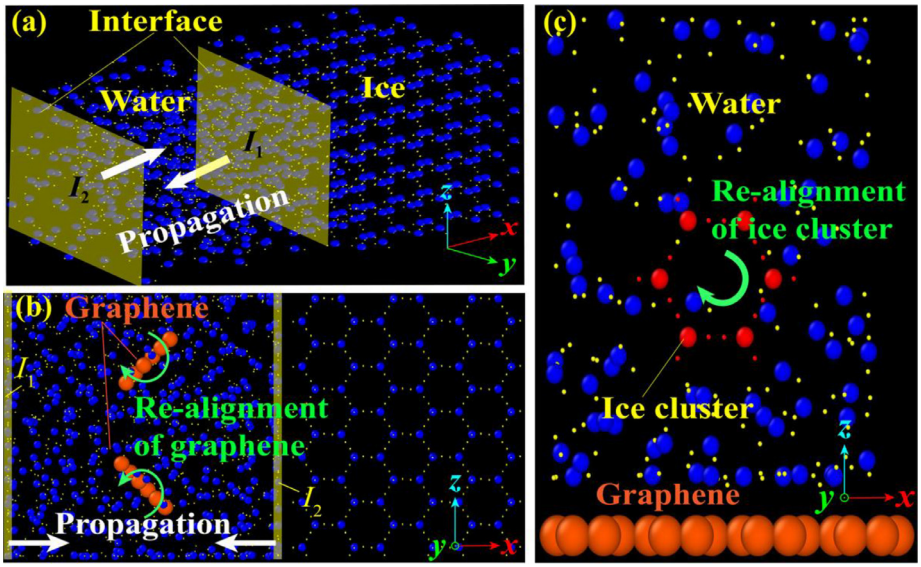

Fig. 1. Initial atomic configurations of molecular dynamics simulations for (a) pure water freezing, (b) water freezing with movable graphene flakes, and (c) water freezing with a movable rigid ice cluster and a graphene plate at bottom. (Blue and yellow spheres: oxygen and hydrogen atoms from water or ice molecules, orange spheres: carbon atoms from graphene, and red spheres: oxygen and hydrogen atoms from the rigid ice cluster).

achieved by the surface interaction and ice crystal surface orientation at the interface as well as temperature.

Although water freezing behaviors have been studied for both pure water [11] and water-surface systems [19], the detailed mechanism of ice propagation and freeze casting process has not been identified clearly to the best of our knowledge. To find an effective control of ice propagation based on fundamental understanding of freezing process, we investigated the water-ice phase change under various conditions, changing temperature, ice crystal orientation, and surface interaction. In this research, molecular dynamics (MD) simulations were employed to address the atomic-scale interactions and structures for the fundamental understanding. For the study of surface interaction, graphene was used as a surface material due to our interest in freeze casting of graphene aerogel for the development of electrode material with effective ion transport and its 2D nature that reduces computational cost and facilitates the analysis.

2. Methodology

Pure water structures were simulated via MD to examine the effects of temperature and ice crystalline structure (Fig. 1a), while the simulated systems for the study of surface interaction included graphene flakes or surface (Figs. 1b and 1c). Since the spontaneous ice nucleation from pure water requires a prohibitively large amount of simulation time in MD [20], a block of ice was introduced as a nucleation seed into initial simulation cells to accelerate the water-ice interface propagation. Here, initial structures of pure water and water with graphene flakes contain 50% of water molecules as ice, and a small ice seed is added near the graphene surface for water-graphene surface simulations. The periodic boundary conditions were used in all three dimensions. Therefore, in the simulation domain for a half-ice/half-water system, two water-ice interfaces (I_1 and I_2) exist, and they propagate in the opposite directions as in Fig. 1a. Simulations with graphene flakes (Fig. 1b) and those with ice cluster and a graphene plate (Fig. 1c) were conducted to investigate the effects of the surface-water interaction on the structural changes, i.e., re-alignment of ice or graphene structures, during the ice propagation ultimately for enhanced understanding of freeze casting.

The TIP4P/ICE model [21] was employed to calculate positions and momentums of water molecules because it accurately reproduces thermodynamic properties, especially ice-water phase change properties. TIP4P/ICE is a rigid water model that fixes bond length (O–H) of 9.572 Å and bond angle (H–O–H) of 104.52° as constant, and the charges of O and H atoms are $-1.179e_c$ and $0.589e_c$, respectively, where e_c is the elementary charge. The massless charge site M was introduced 0.1577 Å away from the O atom. The SHAKE algorithm [22] was also used to enforce the rigidity of water molecules. The particle-particle particle-mesh (PPPM) algorithm [23] is applied to compute the long-range Coulombic interactions among the water molecules. In addition to the Coulombic interaction, dispersive intramolecular interactions (ϕ) between oxygen atoms of water molecules with a distance less than the cut-off distance (r_c) are calculated using the 12–6 Lennard-Jones (LJ) model [24]:

$$\phi(r) = 4\varepsilon\left[\left(\frac{\sigma}{r}\right)^{12} - \left(\frac{\sigma}{r}\right)^{6}\right],\ r \le r_c, \tag{1}$$

where ε is the LJ interaction energy strength, σ is the distance at which the potential is zero, and r is the interatomic distance. In the simulations, the parameters for oxygen-oxygen interaction (O–O) were set as $\varepsilon_{\text{o-o}} = 9.142$ meV, $\sigma_{\text{o-o}} = 3.16$ Å, and $r_{c,\text{o-o}} = 8.5$ Å. In the simulations including graphene, the carbon-oxygen (C–O) interaction for the graphene-water interaction was also calculated using a LJ model with parameters of $\varepsilon_{\text{c-o}} = 8.19$ meV, $\sigma_{\text{c-o}} = 3.19$ Å, and $r_{c,\text{c-o}} = 8.0$ Å [25]. The carbon-carbon (C–C) interaction within a graphene plate was modeled with the Tersoff potential [26].

To integrate Newton's equations of motion, the velocity-Verlet algorithm [27] was used, and the temperatures were controlled via Nose-Hoover thermostats in all MD simulations in this research. Pure water simulations used a time step of 1.0 fs, while simulations with graphene employed a shorter time step (0.5 fs) to treat carbon atoms with high vibrational frequencies. Two different sizes of water freezing simulations containing 864 and 9216 water molecules were conducted to verify the size effect on the simulation results. Moreover, since the triggering of the freezing process varies with surface-to-volume ratio [28], these two systems were adjusted to have the same ratio between the area of water-ice interface and the volume of ice. The result shows that the increment of propagation speed is relatively small (< 14%) with more than 10

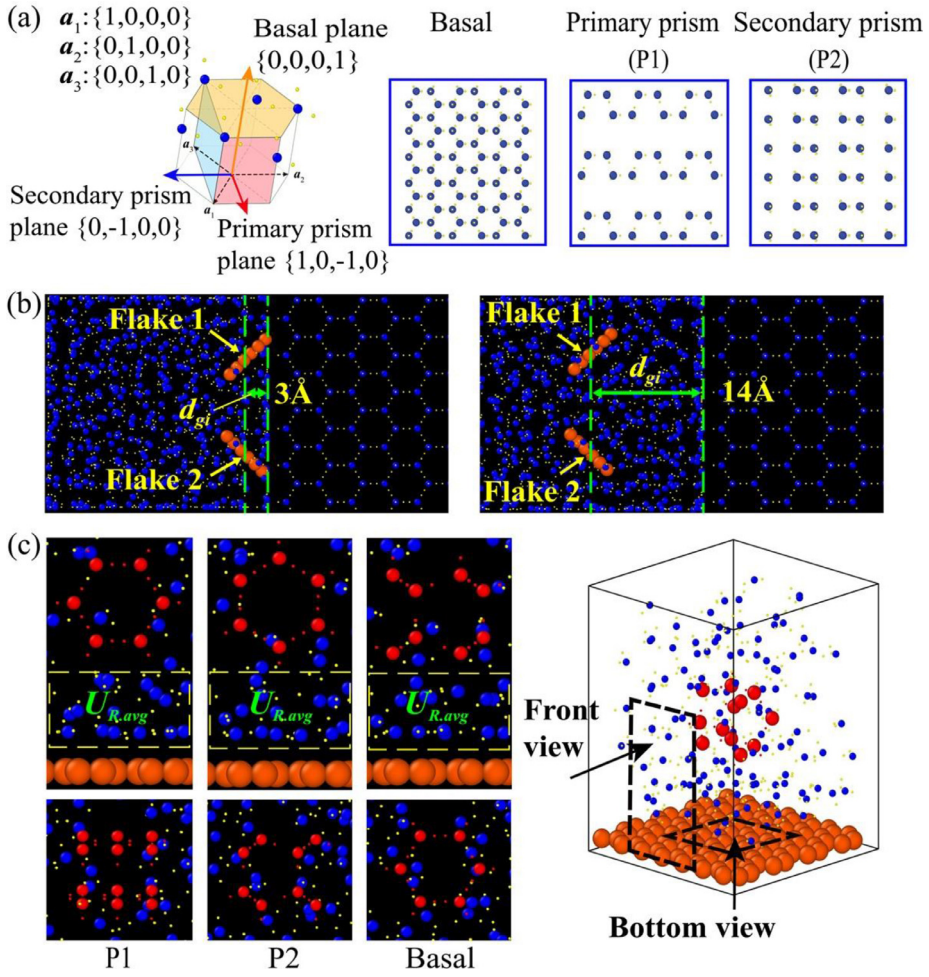

Fig. 2. (a) Hexagonal ice crystal structure and basis vectors, and atomic configurations of three surface orientations (basal, primary prism, and secondary prism). (b) Initial atomic structures (oxygen: blue, hydrogen: yellow, and carbon: orange) of water-ice system with two inclined graphene flakes with two distances (d_{gi}) between the flakes and a water-ice interface, and (c) water with ice seed (red) on graphene surface (first row: front view and second row: bottom view). Three different surfaces of the ice crystals are facing down to graphene.

times larger system size. This result is in a good agreement with a previous study [29].

In MD simulations, temperature, ice crystal orientation, and water-surface interaction were control parameters, and their effects on water-ice interface propagation were investigated. First, to examine the temperature dependence, a 52 Å × 21 Å × 27 Å water-ice system was initially equilibrated at 250 K with an *NPT* ensemble (i.e., fixed number of molecules, pressure, and temperature) for 3.5 ns. After initial relaxation, the ensemble was switched to *NVT* (constant number of molecules, volume, and temperature) at a desired temperature (T) ranging from 200 K to 270 K for 30 ns. The effect of ice crystal orientation was studied by simulating three cases of ice-water system with a different interface structure. Within a simulation box of 52 Å × 21 Å × 27 Å, the ice surface in contact with water has a crystal structure of either basal plane, primary prism plane (denote as P1), or secondary prism plane (denote as P2) as depicted in Fig. 2a. For the analysis of ice propagation, we processed 20 ns of atomic data produced by MD simulations with *NVT* at 250 K, after the relaxation of the initial structures with different ice surface orientations for 1.0 ns (*NPT*, at 250 K).

For the study of the surface interaction, specifically graphene-water interaction, two types of MD simulations were performed. First, water-ice structures that included graphene flakes were used as initial structures to examine the structuring during the freezing process. Two graphene flakes were added to the half-water, half-ice system with a dimension of 52 Å × 21 Å × 27 Å. The distance between the centers of the graphene flakes was 13.3 Å and they have ±45° of inclination angles. Two different distances between the flakes and water-ice interface (d_{gi} = 3 and 14 Å) are set as Fig. 2b shows. The atomic data for analysis were recorded for 30 ns of a simulation with *NVT* at 220 K, and we examined the relative orientation between the graphene flakes and the basal plane of the ice crystal. The second case of freezing simulations with graphene-water interaction employed initial atomic structures of 17 Å × 17 Å × 22 Å water with a 17 Å × 17 Å graphene surface. A prebuilt ice seed of 4.5 Å × 5.2 Å × 4.6 Å was included, and the center of the ice seed was located 9.7 Å above the graphene surface. Three different crystal orientations of the ice seed surface (i.e., primary prism, secondary prism, and basal) facing the graphene were tested in MD as in Fig. 2c. The atomic trajectory data from the MD simulations (with *NVT* at 220 K) for 100 ns were used for the analysis of ice propagation and atomic behaviors during freezing. For the study of energetics during freezing, the regional energies of the three configurations ($U_{R,avg}$) were calculated from the potential energy of water molecules in the sampling region, which was defined between the ice cluster and graphene flakes (yellow dash line in Fig. 2c).

Since we studied effective control of ice propagation, the propagation speed was a major property that we measured by pro-

cessing the resulting MD data. The speed was calculated using the location change of the water-ice interface with respect to time. To identify the phase (water or ice) and ultimately the location of the water-ice interface, we employed the Steinhardt-Nelson order parameter (q) [30]. This method quantitatively recognizes specific crystal orders based on spherical harmonic functions Y_{lm} [31], which are the solutions of the Laplace's equation in the spherical domains and widely used to describe spherical or near-spherical symmetry systems. Each Y_{lm}, where l and m stand for the orders of the functions, represents a specific shape of the solution. The Steinhardt-Nelson order parameter of order l of molecule i is given as,

$$q_l(i)=\sqrt{\frac{4\pi}{2l+1}\sum_{m=-l}^{+l}|q_{lm}(i)|^2},$$

$$\text{where } q_{lm}(i)=\frac{1}{n_{NN}(i)}\sum_{j=1}^{n_{NN}(i)}Y_{lm}\left(\boldsymbol{r}_{ij}\right),\ j\neq i. \tag{2}$$

Here, $\boldsymbol{r}_{ij}$ represents a position vector from molecule i to j (represented by O atom), and $n_{NN}(i)$ is the total number of the nearest neighboring molecules of i. Using the structure order parameters of molecule i and its nearest neighboring molecules, the average structure order parameter $\bar{q}_l(i)$ is calculated as [32]

$$\bar{q}_l(i)=\sqrt{\frac{4\pi}{2l+1}\sum_{m=-l}^{l}|q_{lm}(i)|^2},$$

$$\text{where } \bar{q}_{lm}(i)=\frac{1}{n_{NN}(i)+1}\sum_{j=1}^{n_{NN}(i)+1}q_{lm}(j). \tag{3}$$

Water molecules with the average Steinhardt-Nelson parameter of order 6 larger than 0.385 ($\bar{q}_6 > 0.385$) are recognized as ice-like phase, while those with $\bar{q}_6 < 0.385$ are as water-like phase [32]. For ice-like structures ($\bar{q}_6 > 0.385$), $\bar{q}_4$ is used to identify a more detailed structure order; i.e., when $\bar{q}_4 < 0.42$, the ice structure is regarded as hexagonal (ice-I_h), while it is cubic for $\bar{q}_4 > 0.42$ (ice-I_c). Thus, the $\bar{q}_6$-$\bar{q}_4$ scatter plot was used to analyze the freezing progress and the detailed ice crystal structure. For the calculation of the water-ice interface propagation speed u_{wi}, the entire simulation domain of the water-ice system was subdivided into n slabs (S_k, k = 1, 2, 3, ..., n) with a uniform thickness of 4.2 Å along the x-axis (ice propagation direction). Local structure order parameter ($\bar{q}_{6,k}$) at $x = x_k$ (the center location of slab k) was evaluated by taking an ensemble average of $\bar{q}_6$ of water molecules in slab k. Using the spatial distribution of local structure order parameter $\bar{q}_{6,k}$ and the ice-water criterion for $\bar{q}_6$, the location of the water-ice interface was identified. Since the freezing propagation accelerates as the liquid volume shrinks, the calculation of u_{wi} excluded the freezing of the last two slabs before the freezing completion of the whole simulation domain.

To understand detailed mechanisms of ice propagation control, we examined the thermodynamic driving force of water-ice phase change, the mobility of water molecules to join the phase transition, and the interfacial energetics. These are characterized by calculating i) the difference of free energy between water and ice phases, ΔG (eV), ii) self-diffusivity of water molecules, D (m^2/s), and iii) water-ice interfacial energy γ_{wi} (mJ/m^2) [33], respectively. Using the free-energy perturbation (FEP) method [34], the free-energy difference (ΔG) between state A and state B was calculated as

$$\Delta_A^B G=-k_BT\ln\left\langle\exp\left(-\frac{U_B-U_A}{k_BT}\right)\right\rangle \tag{4}$$

where k_B is Boltzmann's constant (8.617×10^{-5} eV/K), and U_A and U_B are the potential energies of the system at state A and state B, respectively, and the angle brackets represent an ensemble average. In MD, the free-energy perturbation is applied by coupling a perturbation parameter λ into the interaction force calculation, varying λ from 0 to 1 with an increment of $d\lambda = 0.001$. The perturbation parameter λ was introduced into the atomic point charges of oxygen and hydrogen atoms ($\lambda = 0$ for no charge, while $\lambda = 1$ for full charge). Therefore, the free energy (G) in this study was determined as overall free-energy difference $\Delta_{\lambda=0}^{\lambda=1}G$, which was obtained from the ensemble average (over 10,000 cases for each λ) of the free-energy difference from timestep i to $i+1$:

$$\Delta_{\lambda=0}^{\lambda=1}G=\sum_{i=0}^{n-1}\Delta_{\lambda_i}^{\lambda_{i+1}}G=-k_BT\sum_{i=0}^{n-1}\ln\left\langle\exp\left(-\frac{U_{i+1}-U_i}{k_BT}\right)\right\rangle,\ i=1\cdots n, \tag{5}$$

where n is the total number of the timesteps during the simulation.

The self-diffusivity can be calculated by taking the mean square displacement (MSD) of the simulated molecules [35, 36]:

$$\text{MSD}(t)=\langle\Delta\boldsymbol{r}(t)^2\rangle=\frac{1}{N}\sum_{i=1}^{N}[\boldsymbol{r}_i(t)-\boldsymbol{r}_i(0)]^2, \tag{6}$$

where $\boldsymbol{r}_i(t)$ is the position vector of oxygen atom i at time t. Using the time dependence of MSD(t), the self-diffusivity (D) is given as,

$$D=\lim_{t\to\infty}\frac{\text{MSD}(t)}{6t}. \tag{7}$$

With the calculated D, the diffusion activation energy of supercooled water can be obtained by fitting D with respect to temperature to the Arrhenius expression [37]:

$$D=D_0\exp\left(-\frac{Q_v}{k_BT}\right), \tag{8}$$

where D_0 is pre-exponential factor, and Q_v is the activation energy (eV). To estimate the dependence of the diffusivity on temperature, a series of MD simulations of supercooled pure water systems (with 432 water molecules included) were conducted at T = 200 – 270 K.

Unlike the free-energy difference and the diffusivity, the water/ice interfacial energy (γ_{wi}) is independent of temperature [38]. The calculation of γ_{wi} employed the ensemble switch method [39], where the energy difference between two different ensemble stages is calculated. In the first stage, two separate ice and water systems are simulated under the periodic boundary conditions in all directions. The total energies of ice-only and water-only simulation structures were measured under equilibrium and denoted as E_w and E_i, respectively. Then, combining the water and ice systems, the total energy E_{w+i} of the combined systems was calculated and compared with that from the separate systems. Therefore, the interfacial energy γ_{wi} is given by

$$\gamma_{wi}=\frac{E_{w+i}-(E_w+E_i)}{2A}, \tag{9}$$

where A is the area of water-ice interface.

3. Results and discussion

3.1. Ice propagation in pure water

During freezing, new layers of crystal ice are formed near the water-ice interface until the entire system is frozen. As depicted in Fig. 3a, the water-ice interfaces (I_1 and I_2) were propagated, expanding the crystal ice region between 0 and 30 ns af-

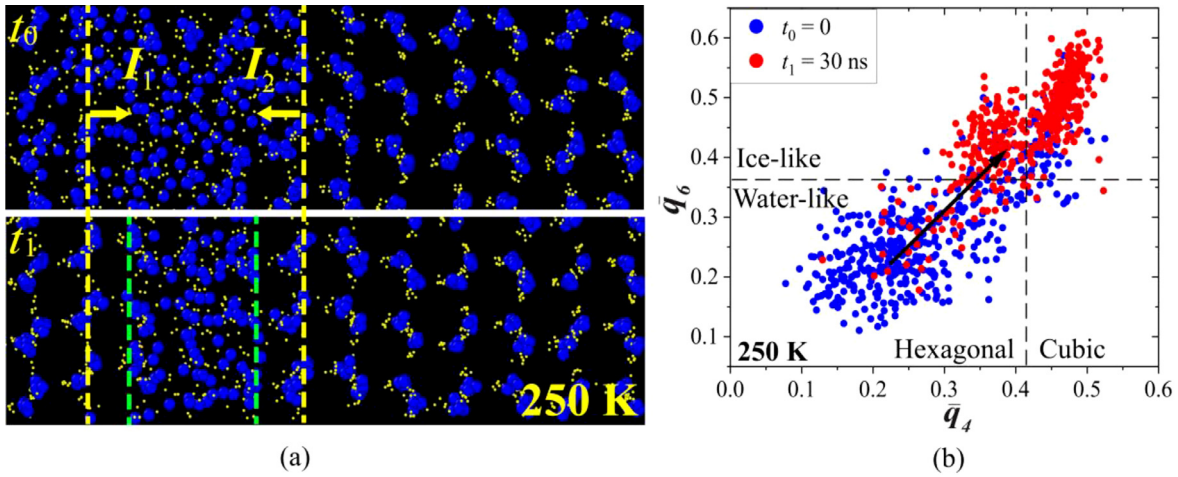

Fig. 3. The freezing process of water-ice system at 250 K: (a) the water-ice interfaces propagate from ice region toward water region, and (b) the structure order parameter plot at two different time steps, ($t_0 = 0$; $t_1 = 30$ ns after freezing process). More molecules have structure order parameters $\bar{q}_6$ larger than the water-ice criterion of 0.385 at $t = t_1$, demonstrating the formation of hexagonal ice structure.

ter relaxation. The scatter plot of structure order parameters of water molecules in the entire simulation domain quantitatively confirms the expansion of ice crystal (Fig. 3b), i.e., more data points or more molecules of local order parameter $\bar{q}_6 > 0.385$ at $t = 30$ ns.

To examine the water-ice propagation speed under different temperature below the freezing point of the system, the supercooling temperature is defined as $\Delta T_{sc} = T_m - T_{sys}$, where T_m is the water-ice phase change temperature in MD simulations (265 K in this study) and T_{sys} is the simulated system temperature. In pure water-ice systems, the water-ice interface propagation speed (u_{wi}), which was estimated by averaging the propagation speed from three crystal surfaces (P1, P2, and basal), reached the maximum (0.20 m/s) at 13 K of ΔT_{sc} (denoted as $\Delta T_{sc,\max}$), as shown in Fig. 4a. When the supercooling temperature is lower than $\Delta T_{sc,\max}$, u_{wi} decreased with decreasing ΔT_{sc}, while for $\Delta T_{sc} > \Delta T_{sc,\max}$, u_{wi} increased with decreasing ΔT_{sc}. In the simulations, significant water-ice interface propagation (0.02 m/s to 0.20 m/s) was observed in the range of 3 – 25 K of ΔT_{sc}. The supercooling and the maximum propagation from our simulations ($u_{wi} = 0.20$ m/s at 13 K of ΔT_{sc}) are in good agreements with other MD works [11, 40] and experimental works [41], as presented in Fig. 4a. Even though the maximum propagation speed appears at larger ΔT_{sc} in the experimental work [41, 46], the overall dependence and speed are similar to our study.

The number of water molecules in an ice-like structure ($\bar{q}_6 > 0.385$) at 30 ns after the beginning of ice propagation was the largest at $\Delta T_{sc,\max}$ (= 13 K), while at 65 K of ΔT_{sc}, transition to ice structure in the initial water region was not observed (Fig. 4b). Large fraction of newly formed ice structures, when the highest propagation speed appears (i.e., at $\Delta T_{sc,\max} = 13$ K), are cubic-like, while the hexagonal ice structures are created partially in case of $\Delta T_{sc} = 5$ K with a lower propagation speed. This is attributed to a rapid phase transformation at $\Delta T_{sc,\max}$ which causes the metastable phase of ice (ice-I_c). On the other hand, the lower propagation speed provides water molecules with sufficient time for transition to more stable phase, i.e., hexagonal ice structure (ice-I_h) [47].

To explain the dependency of u_{wi} on the temperature (T_{sys}), the mobility of water molecules and thermodynamic driving force of water-ice phase change were examined by calculating the self-diffusivity D and the free-energy difference between water and ice (ΔG) at several temperatures. The self-diffusivity D describes the random translational movement of water molecules driven by the internal kinetic energy [48]. Fig. 4c shows the self-diffusivity D of supercooled water calculated using MD data in a temperature range of 200 – 280 K, and the results are compared with experiments [42]. Although the self-diffusivities from MD are around five times smaller than the experiments, the MD activation energy (−35.82 kJ/mol) that was calculated from the temperature-dependence of the self-diffusivity between 200 K and 270 K is close to the value determined by the experiment (−30.16 kJ/mol) from 240 K to 270 K. The discrepancy from the experiments can originate from the size effect in molecular simulations or the usage of rigid water model, where atomic movements are constrained [49]. The appearance of the maximum u_{wi} at higher temperatures (smaller supercooling) in MD than experiments can be attributed to the lower of self-diffusivity in MD, as Fig. 4a presents. Since temperature represents the average kinetic energy of water molecules, lower temperatures lead to lower mobilities or smaller self-diffusivity. The lower mobilities of water molecules slow the ice propagation as the transition to ice requires the migration of water molecules to a lattice point of the ice crystal.

While the mobility of water molecules increases with temperature, the thermodynamic driving force of the phase change, which we characterized using the free-energy difference between supercooled water and ice, decreases with increasing temperature, as Fig. 4d shows. Linear fitting and extrapolation of the free-energy values from MD simulations indicate that the free energy of crystal ice is less than that of water when $T_{sys} < 280$ K, which confirms that ice is more energetically stable. The opposite temperature dependences of the thermodynamic driving force and self-diffusivity of water molecules explain the existence of optimum freezing temperature ($T_{wi,\max}$) for the maximum water-ice propagation speed (252 K in this report).

The water-ice interface propagation speed (u_{wi}) also depends on the orientation of ice crystal surface that contacts water as shown in Fig. 5a and b. When the secondary plane (P2) of ice crystal is in contact with liquid water, the water-ice interface propagation is the fastest in all ranges of ΔT_{sc} (Fig. 5a), while the basal plane-water interface have the slowest propagation speed. The energy analysis (Fig. 5b) also shows that a larger water-ice interfacial energy (γ_{wi}) was measured in case of faster propagation speed; P2-water interface has the largest γ_{wi}, and the basal plane-water interface has the lowest. Since a lower interfacial energy represents a more stable configuration, which leads to a lower atomic mo-

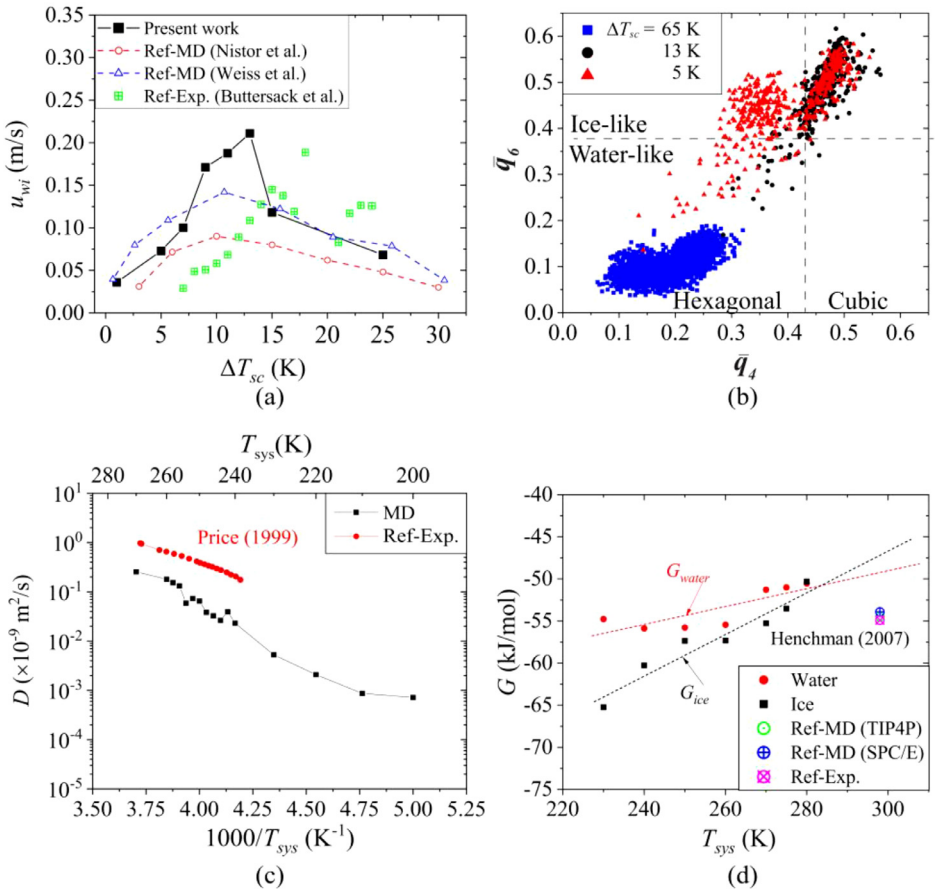

Fig. 4. (a) The water-ice interface propagation speed (u_{wi}) averaged over three crystal orientations with respect to the supercooling temperature (ΔT_{sc}). The red open circles and blue open triangles represent the results of ice propagation speed from other MD studies [11, 40], and the green cross rectangles do those from a previous experimental study [41]. (b) The distributions of the structure order parameters ($\bar{q}_4$ and $\bar{q}_6$) of water molecules in the water-side region at three supercooling temperatures, ΔT_{sc} = 65 (blue squares; T_{sys} = 200 K), 13 (black circles; 252 K), and 5 K (red triangles; 260 K) after 30 ns of freezing propagation. (c) Self-diffusivity (D) and (d) free energy of supercooled water and ice (G_{water} and G_{ice}) with respect to the temperature. The results are compared with experimental self-diffusivities [42] and free energy from MD with the TIP4P water model [43], MD with the SPC/E model [44], and experiments [45].

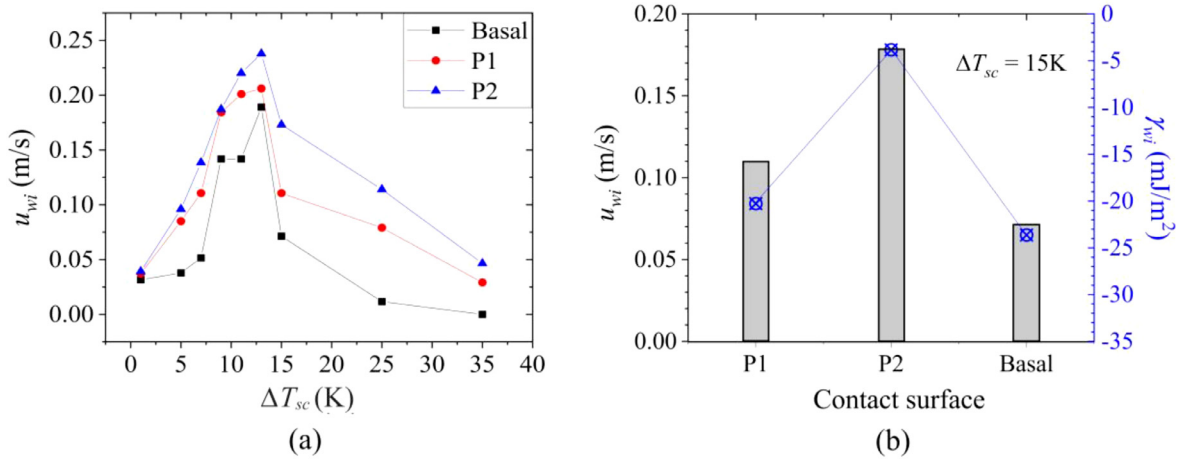

Fig. 5. (a) Temperature dependency of propagation speed from different crystal orientations at interface. (b) Speed of water-ice interface propagation (u_{wi}; gray bars) and interfacial energy (γ_{wi}; blue crossed circles) for the three different orientations at 15 K of ΔT_{sc}.

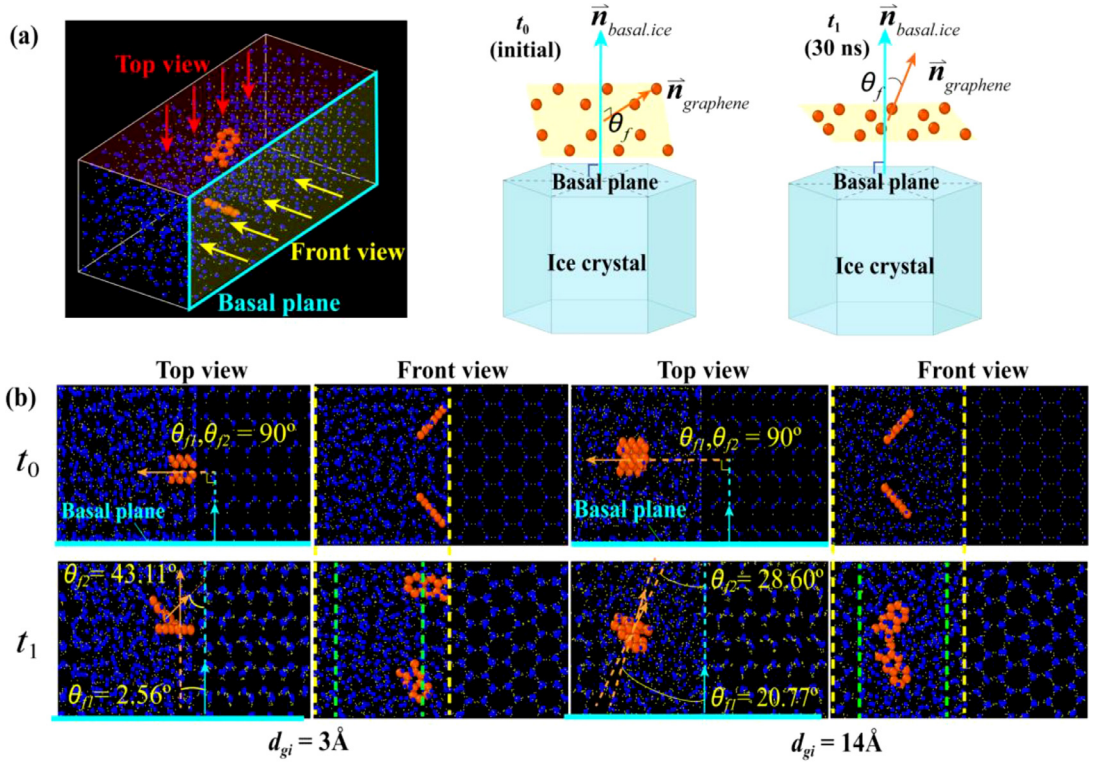

Fig. 6. (a) Schematic illustration of the angle between graphene and basal plane normal vector. (Cyan surfaces and arrows: basal plane and its normal vector, orange arrows: normal vector of graphene flake surfaces) (b) Change of the alignment of two graphene flakes during the freezing process between $t_0 = 0$ and $t_1 = 30$ ns. The crystal surface of the interface is secondary prism plane (P2).

Table 1
Angles between the graphene flakes and the basal plane of ice crystal ($\theta_{f,1}$ and $\theta_{f,2}$) at $t_1 = 30$ ns for two different distances between the graphene flake and water-ice interface ($d_{gi} = 3$ and 14 Å).

d_{gi} (Å)	$\theta_{f,1}$	$\theta_{f,2}$
3	2.56 °	43.11°
14	20.77°	28.60°

bility and slower ice propagation [50], the dependence of freezing propagation speed on the water-ice interface orientation can be attributed to the interfacial energy.

3.2. Effects of water-graphene interaction

The effects of surface-water interactions on water phase change process, in addition to pure water properties discussed in Section 3.1, were examined for the understanding of freeze casting. In the freezing simulations of water with graphene flakes for the study of surface interaction effects, all the surfaces of graphene flakes were initially perpendicular to the basal plane of the ice crystal, i.e., angle between graphene and basal plane normal vector, θ_f is 90°, as in Fig. 6a. However, due to the water-graphene interactions, as ice propagates near graphene surface, all the graphene flakes rotated about the long axis of the flakes, reducing the angles with the basal plane ($\theta_{f,1}$ and $\theta_{f,2}$, where 1 and 2 are index of the flake) as in Fig. 6b. The change of the angle between graphene flakes and the ice crystal basal plane are summarized in the Table 1. Two cases of the simulations with different distances between flakes and the water-ice interface ($d_{gi} = 3$ and 14 Å) show that the larger distance case resulted in the re-arrangement of two graphene flakes with more similar degrees of the flake-basal plane angle.

The preferred parallel angle between graphene surface and ice crystal basal plane was also observed in the simulations with a large graphene surface. Even with a different initial orientation of ice seed as described in Fig. 2c, the ice cluster ended up with the basal plane parallel to the graphene surface as shown in Fig. 7a and b. Thus, for the first two cases of initial ice cluster orientations, where a primary or secondary prism plane (P1 and P2) of ice cluster is parallel to the graphene surface, the ice cluster rotated to have the basal plane facing down.

As Fig. 7c shows, the initial potential energy ($U_{R.avg}$) of the ice cluster-graphene interfacial region is −1.84 eV when the basal plane faces the graphene surface, and it is lower than the other two cases ($U_{R.avg} = -0.31$ eV for the primary prism plane and −0.51 eV for the secondary prism plane). During the freezing process, the $U_{R.avg}$ from the first two cases (P1 and P2 plane facing the graphene surface) gradually decreased as the ice cluster rotated to have the basal plane parallel to the surface. Consequently, the $U_{R.avg}$ from three different orientation cases converged to a similar value (~ -2.0 eV at $t_1 = 100$ ns). As the lower $U_{R.avg}$ represents the more stable configuration, the configuration where the basal plane and graphene are parallel is the most stable. This explains the alignment of graphene flakes in Fig. 6 and the ice cluster rotation of the P1 and P2 cases in Fig. 7. Moreover, after the alignment of the ice cluster for the basal plane parallel to graphene, the hexagonal structure of water molecules started forming around the ice cluster, showing ice growth. As discussed above in Fig. 5, the ice crystal mainly grows in a direction normal to the P2 or P1 plane, i.e., parallel to the basal plane. Therefore, with graphene-water surface interactions, ice mainly grows in a direction parallel to graphene surface.

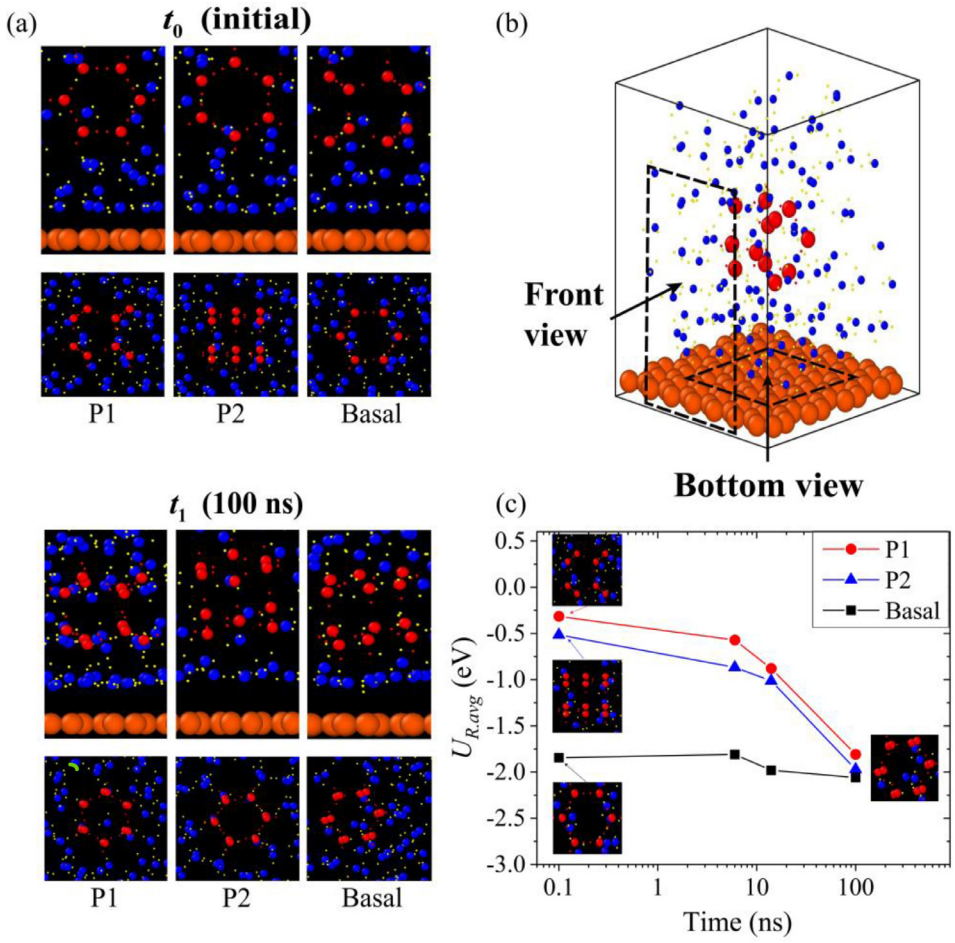

Fig. 7. (a) Atomic configurations from the bottom view of water freezing simulations with graphene surface (orange) and three different initial orientations of ice cluster (red) at $t_0 = 0$, and $t_1 = 100$ ns. First and third row: front view, second and fourth row: bottom view. (b) Schematic illustration describes the viewing direction of the front and bottom view. (c) Regional potential energy ($U_{R.avg}$) of three cases of different ice cluster orientations.

4. Conclusions

In this research, the fundamental controlling mechanisms of water-ice interface propagation were investigated through molecular dynamics. The maximum propagation speed of the water-ice interface appeared at 252 K. The competition between self-diffusivity and thermodynamic driving force results in an optimal temperature for maximum ice growth speed. Water-ice interfacial energy depends on the orientation of water-contacting ice surface, and a higher interfacial energy leads to a faster ice propagation speed. Thus, the ice propagation speed depends on water-ice surface orientation. Graphene-water surface interactions align ice clusters or graphene flakes to have a minimum energy state, in which the basal plane of the ice crystal is parallel with the graphene surface. As a result, the orientation of ice crystals and the ice growth speed and direction can be changed by controlling surface interactions. This study provides insights to ice propagation control mechanisms for effective freeze cast structuring and its broader applications.

Declaration of Competing Interest

The authors declare that they have no known competing financial interests or personal relationships that could have appeared to influence the work reported in this paper.

CRediT authorship contribution statement

Yu-Kai Weng: Methodology, Software, Validation, Formal analysis, Investigation, Data curation, Writing – original draft, Visualization. **Seungha Shin:** Conceptualization, Methodology, Writing – original draft, Writing – review & editing, Funding acquisition, Project administration, Supervision. **Kenneth D. Kihm:** Funding acquisition, Writing – review & editing. **Mohammad Bahzad:** Writing – review & editing. **Douglas S. Aaron:** Funding acquisition, Writing – review & editing.

Acknowledgement

The authors gratefully acknowledge the financial support by the U.S. National Science Foundation (Grant No. CBET-1933800). This work utilized the resources of Extreme Science and Engineering Discovery Environment (XSEDE), which is supported by National Science Foundation Grant number ACI-1053575.

References

[1] S. Hirano, C. Upper, Bacteria in the leaf ecosystem with emphasis on pseudomonas syringae-a pathogen, ice nucleus, and epiphyte, Microbiol. Mol. Biol. Rev. 64 (2000) 624–653.
[2] T. Koop, B.J. Murray, A physically constrained classical description of the homogeneous nucleation of ice in water, J. Chem. Phys. 145 (21) (2016) 211915.
[3] A. Michaelides, K. Morgenstern, Ice nanoclusters at hydrophobic metal surfaces, Nat. Mater. 6 (8) (2007) 597–601.

[4] K.L. Scotti, D.C. Dunand, Freeze casting – a review of processing, microstructure and properties via the open data repository, FreezeCasting.net, Prog. Mater Sci. 94 (2018) 243–305.
[5] G. Shao, D.A.H. Hanaor, X. Shen, A. Gurlo, Freeze casting: from low-dimensional building blocks to aligned porous structures - a review of novel materials, methods, and applications, Adv. Mater. 32 (17) (2020) 1907176.
[6] H. Bai, Y. Chen, B. Delattre, A.P. Tomsia, R.O. Ritchie, Bioinspired large-scale aligned porous materials assembled with dual temperature gradients, Sci. Adv. 1 (11) (2015) e1500849.
[7] H.-.L. Gao, Y.-.B. Zhu, L.-.B. Mao, F.-.C. Wang, X.-.S. Luo, Y.-.Y. Liu, Y. Lu, Z. Pan, J. Ge, W. Shen, Y.-.R. Zheng, L. Xu, L.-.J. Wang, W.-.H. Xu, H.-.A. Wu, S.-.H. Yu, Super-elastic and fatigue resistant carbon material with lamellar multi-arch microstructure, Nat. Commun. 7 (1) (2016) 12920.
[8] M.C. Gutiérrez, Z.Y. García-Carvajal, M.J. Hortigüela, L. Yuste, F. Rojo, M.L. Ferrer, F. del Monte, Biocompatible MWCNT scaffolds for immobilization and proliferation of E. coli, J. Mater. Chem. 17 (29) (2007) 2992–2995.
[9] T. Zhai, X. Lu, H. Wang, G. Wang, T. Mathis, T. Liu, C. Li, Y. Tong, Y. Li, An Electrochemical capacitor with applicable energy density of 7.4Wh/kg at average power density of 3000W/kg, Nano Lett. 15 (5) (2015) 3189–3194.
[10] A.Z. Lichtner, D. Jauffrès, C.L. Martin, R.K. Bordia, Processing of hierarchical and anisotropic porosity LSM-YSZ composites, J. Am. Ceram. Soc. 96 (9) (2013) 2745–2753.
[11] V.C. Weiss, M. Rullich, C. Köhler, T. Frauenheim, Kinetic aspects of the thermostatted growth of ice from supercooled water in simulations, J. Chem. Phys. 135 (3) (2011) 034701.
[12] P. Montero de Hijes, J.R. Espinosa, C. Vega, E. Sanz, Ice growth rate: temperature dependence and effect of heat dissipation, J. Chem. Phys. 151 (4) (2019) 044509.
[13] D. Rozmanov, P. Kusalik, Temperature dependence of crystal growth of hexagonal ice (I-h), PCCP 13 (2011) 15501–15511.
[14] J. Liu, C. Zhu, K. Liu, Y. Jiang, Y. Song, J. Francisco, Z. Cheng, J. Wang, Distinct ice patterns on solid surfaces with various wettabilities, Proc. Natl. Acad. Sci. 114 (43) (2017) 11285–11290.
[15] G. Algara-Siller, O. Lehtinen, F.C. Wang, R.R. Nair, U. Kaiser, H.A. Wu, A.K. Geim, I.V. Grigorieva, Square ice in graphene nanocapillaries, Nature 519 (7544) (2015) 443–445.
[16] A. Akaishi, T. Yonemaru, J. Nakamura, Formation of water layers on graphene surfaces, ACS Omega 2 (5) (2017) 2184–2190.
[17] S. Chen, A.P. Draude, A.X.C. Nie, H.P. Fang, N.R. Walet, S. Gao, J.C. Li, Effect of layered water structures on the anomalous transport through nanoscale graphene channels, J. Phys. Commun. 2 (8) (2018) 085015.
[18] J. Hayward, A. Haymet, The ice/water interface: molecular dynamics simulations of the basal, prism, {202±}, and {21±°} interfaces of ice Ih, J. Chem. Phys. 114 (2001) 3713–3726.
[19] Z. Gao, N. Giovambattista, O. Sahin, Phase diagram of water confined by graphene, Sci. Rep. 8 (1) (2018) 6228.
[20] M. Matsumoto, S. Saito, I. Ohmine, Molecular dynamics simulation of the ice nucleation and growth process leading to water freezing, Nature 416 (6879) (2002) 409–413.
[21] J.L.F. Abascal, E. Sanz, R.G. Fernández, C. Vega, A potential model for the study of ices and amorphous water: TIP4P/Ice, J. Chem. Phys. 122 (23) (2005) 234511.
[22] J.-.P. Ryckaert, G. Ciccotti, H.J.C. Berendsen, Numerical integration of the cartesian equations of motion of a system with constraints: molecular dynamics of n-alkanes, J. Comput. Phys. 23 (3) (1977) 327–341.
[23] R.W. Hockney, J.W. Eastwood, in: Computer Simulation Using Particles, 1st ed, CRC Press, 1988, pp. 367–404.
[24] L.S. Tee, S. Gotoh, W.E. Stewart, Molecular parameters for normal fluids. Lennard-Jones 12-6 potential, Ind. Eng. Chem. Fund. 5 (3) (1966) 356–363.
[25] D.C. Marable, S. Shin, A.Y. Nobakht, Investigation into the microscopic mechanisms influencing convective heat transfer of water flow in graphene nanochannels, Int. J. Heat Mass Transf. 109 (2017) 28–39.
[26] A. Kınacı, J.B. Haskins, C. Sevik, T. Çağın, Thermal conductivity of BN-C nanostructures, Phys. Rev. B 86 (11) (2012) 115410.
[27] L. Verlet, Computer "Experiments" on classical fluids. I. Thermodynamical properties of Lennard-Jones molecules, Phys. Rev. 159 (1) (1967) 98–103.
[28] A. Tabazadeh, Y.S. Djikaev, H. Reiss, Surface crystallization of supercooled water in clouds, Proc. Natl. Acad. Sci. U.S.A. 99 (25) (2002) 15873–15878.
[29] Y. Lü, X. Zhang, M. Chen, Size effect on nucleation rate for homogeneous crystallization of nanoscale water film, J. Phys. Chem. B 117 (35) (2013) 10241–10249.
[30] P. Steinhardt, D. Nelson, M. Ronchetti, Bond-orientational order in liquids and glasses, Phys. Rev. B 28 (2) (1983) 784–805.
[31] S. Auer, D. Frenkel, in: Advanced Computer simulation: Approaches for Soft Matter Sciences I, Springer, Berlin Heidelberg, 2005, pp. 149–208.
[32] W. Lechner, C. Dellago, Accurate determination of crystal structures based on averaged local bond order parameters, J. Chem. Phys. 129 (11) (2008) 114707.
[33] S. Javan Nikkhah, M.R. Moghbeli, S.M. Hashemianzadeh, A molecular simulation study on the adhesion behavior of a functionalized polyethylene-functionalized graphene interface, Phys Chem Chem Phys 17 (41) (2015) 27414–27427.
[34] R.W. Zwanzig, High-temperature equation of state by a perturbation method. I. Nonpolar Gases, J. Chem. Phys. 22 (8) (1954) 1420–1426.
[35] J. Wang, S. Shin, A. Hu, Geometrical effects on sintering dynamics of Cu–Ag core–shell nanoparticles, J. Phys. Chem. C 120 (31) (2016) 17791–17800.
[36] M.A.A. Hasan, J. Wang, Y.C. Lim, A. Hu, S. Shin, Concentration dependence of hydrogen diffusion in α-iron from atomistic perspectives, Int. J. Hydrog. Energy 44 (51) (2019) 27876–27884.
[37] J. Key, D.W. Ball, Introductory Chemistry, 1st Canadian ed, BCcampus, 2014.
[38] Y. Zhang, E. Anim-Danso, S. Bekele, A. Dhinojwala, Effect of surface energy on freezing temperature of water, ACS Appl. Mater. Interfaces 8 (27) (2016) 17583–17590.
[39] P. Virnau, F. Schmitz, K. Binder, The ensemble switch method and related approaches to obtain interfacial free energies between coexisting phases from simulations: a brief review, Mol. Simul. 42 (6–7) (2016) 549–562.
[40] R.A. Nistor, T.E. Markland, B.J. Berne, Interface-limited growth of heterogeneously nucleated ice in supercooled water, J. Phys. Chem. B 118 (3) (2014) 752–760.
[41] T. Buttersack, S. Bauerecker, Critical radius of supercooled water droplets: on the transition toward dendritic freezing, J. Phys. Chem. B 120 (3) (2016) 504–512.
[42] W.S. Price, H. Ide, Y. Arata, Self-diffusion of supercooled water to 238K using PGSE NMR diffusion measurements, J. Phys. Chem. A 103 (4) (1999) 448–450.
[43] R.H. Henchman, Free energy of liquid water from a computer simulation via cell theory, J. Chem. Phys. 126 (6) (2007) 064504.
[44] H.J.C. Berendsen, J.R. Grigera, T.P. Straatsma, The missing term in effective pair potentials, J. Phys. Chem. 91 (24) (1987) 6269–6271.
[45] W. Wagner, A. Pruß, The IAPWS Formulation 1995 for the thermodynamic properties of ordinary water substance for general and scientific use, J. Phys. Chem. Ref. Data 31 (2) (2002) 387–535.
[46] T. Wang, Y. Lü, L. Ai, Y. Zhou, M. Chen, Dendritic growth model involving interface kinetics for supercooled water, Langmuir 35 (15) (2019) 5162–5167.
[47] S.-.H. Guan, C. Shang, S.-.D. Huang, Z.-.P. Liu, Two-stage solid-phase transition of cubic ice to hexagonal ice: structural origin and kinetics, J. Phys. Chem. C 122 (50) (2018) 29009–29016.
[48] S. Mori, J. Zhang, in: Encyclopedia of Neuroscience, Academic Press, Oxford, 2009, pp. 531–538.
[49] I.-.C. Yeh, G. Hummer, System-size dependence of diffusion coefficients and viscosities from molecular dynamics simulations with periodic boundary conditions, J. Phys. Chem. B 108 (40) (2004) 15873–15879.
[50] M. Fitzner, G.C. Sosso, S.J. Cox, A. Michaelides, The many faces of heterogeneous ice nucleation: interplay between surface morphology and hydrophobicity, J. Am. Chem. Soc. 137 (42) (2015) 13658–13669.